Density functional theory investigation of titanium-tungsten superlattices: Structure and mechanical properties

Sven P. Rudin

Density functional theory investigation of titanium-tungsten superlattices: structure and mechanical properties

Sven P. Rudin

Los Alamos National Laboratory, Los Alamos, NM 87545

(Dated: October 25, 2012)

Titanium (Ti) exhibits the body-centered crystal structure only at high temperatures. The temperature range of this so-called β-Ti phase can be expanded by alloying Ti with tungsten (W). Rather than placing the W atoms in the β-Ti crystal at random, this work applies density functional theory calculations to explore the consequences of an orderly placement in Ti/W superlattice structures. In all examples the W layer remains bcc-like. The stacking direction of the Ti/W superlattice drives the core of the Ti layer toward either a locally hcp- or ω-Ti structure, though the latter is mechanically unstable for all but the thinnest W layers. The relative thicknesses of the W and Ti layers as well as the stacking direction influence the formation energies, which consistently fall within a range corresponding roughly to room temperature. Superlattices allow a choice of stacking direction and layer thicknesses; both strongly influencing the material's strength, though not improving the mechanical properties as observed for Ti with randomly placed W particles.

I. INTRODUCTION

The phase diagrams of nearly all early transition metal elements feature the body-centered cubic (bcc) crystal structure, either by itself or as one among several solid phases.[1] Titanium (Ti) serves as a prototype among those elements that exhibit the bcc crystal structure only at high temperatures (β-Ti). The α-Ti phase with a hexagonal close-packed (hcp) crystal structure dominates at low temperatures, while the hexagonal ω-Ti phase appears upon compression. The transformation from the bcc to the ω crystal structure can be described by a phonon mode,[2] that from bcc to hcp couples a phonon mode with a shearing of the crystal.[3]

The temperature range of the β-Ti phase can be expanded by alloying Ti with specific elements, termed β-stabilizers. This allows for an increased role in applications benefitting from the phase's low elastic modulus and superior corrosion resistance, e.g., biomedical applications.[4] Similarly, α stabilizers can expand the temperature range of the much stronger α phase. Ti alloys that are extensively used in aerospace and other applications combine both types of stabilizers, along with other elements, to achieve advantageous combinations of strength, corrosion resistance, and machinability.[5] The brittleness of ω-Ti makes it unfavorable,[2] and eliminating its appearance as a retained phase in Ti alloys requires special attention.[6]

Alloying with stabilizers places the impurities at random throughout the lattice. Given that nanometer-scale structures can now be readily prepared, a directed placement of the stabilizers becomes possible and interesting in terms of how it influences properties such as strength. Alternating layers of Ti and the β-stabilizer tungsten (W) in particular, i.e., Ti/W superlattices, have been experimentally realized to study periodic and Fibonacci quasiperiodic superlattices.[7–9] Combining these elements benefits from their bcc phases having close lattice constants, 3.165 Å for bcc W,[10] and 3.311 Å for β-Ti at 1100 °C (extrapolating to 3.27 Å at room temperature).[11] Among the β-isomorphous β-stabilizers, niobium has a lattice constant closer to that of β-Ti with 3.300 Å, but it does not exhibit a surface reconstruction,[12] which W does.[13]

The existence and nature of tungsten's surface reconstruction raises the question of its manifestation at the interfaces in Ti/W superlattices. This surface reconstruction, a structural transition that occurs below room temperature, involves a displacement of atoms in the first few layers near the surface.[14] At high temperatures, the surface atoms appear in truncated bcc positions. Their displacement upon cooling follows the same pattern as exhibited by the atoms in bcc Ti when β-Ti transforms toward α-Ti: a longitudinal surface phonon mode with wave vector $\mathbf{q} = (\pi/a)(1,1)$ for bcc W corresponding to the transverse phonon mode with wave vector $\mathbf{q} = (\pi/a)(1,1,0)$ for bcc Ti. Superlattices of W and Ti could potentially show several interesting possibilities: the W layer could stabilize the Ti layer in a bcc crystal, or the Ti layer could impart a distortion toward hcp into the W layer, aided by the latter's surface reconstruction.

How the Ti and W layers interact depends on the orientation of their interface relative to an initial, common bcc-like structure. Stacking along the [001] direction aligns the W surface reconstruction with the phonon mode that takes bcc Ti to a hcp crystal structure. Stacking along the [011] direction sets the interface perpendicular to the phonon mode. Stacking along the [111] direction places the interface perpendicular to the bcc-to-ω distortion, in which two out of three bcc atomic planes collapse into a single, honeycomb layer interspersed between hexagonal layers.

II. METHOD

The work presented here explores the structural properties of Ti/W superlattices using density functional theory (DFT) calculations. These apply the Vienna Ab initio Simulation Package[15,16] with the projector-augmented wave method[17] in the generalized gradient approximation of Perdew, Burke, and Ernzerhof.[18] Total energies are calculated with a plane wave cutoff energy of 400 eV, a $\mathbf{k}$-point mesh of density 40 Å^{-1}, and the linear tetrahedron method with Blöchl corrections;[19] the self-consistent cycles are converged to 1 μeV. This DFT framework reproduces the experimental lattice constants of bcc Ti and bcc W to within 1%.

The calculations optimize unit cells that initially stack a layer of bcc Ti against a layer of bcc W along high-symmetry directions with $n_{\mathrm{Ti}} + n_{\mathrm{W}}$ monolayers in the stacking direction. Unit cells with a single atom per monolayer allow phonon modes to transform the Ti layer from bcc-like to hcp- or ω-like for [011] or [111] stacking, respectively, though for the [111] stacking direction having a single atom per monolayer proves to be too restrictive (see below). The [001] stacking requires unit cells with two atoms per monolayer to transform the Ti layer from bcc-like to hcp-like. Results presented here focus on systems with $n_{\mathrm{Ti}} + n_{\mathrm{W}} = 18$ monolayers, which is large enough to show the interesting physics without requiring an overwhelming computational effort. An exception appears for phonon calculations, which compare systems with $n_{\mathrm{Ti}} + n_{\mathrm{W}} = 9$ monolayers.

(a) [001] stacking direction

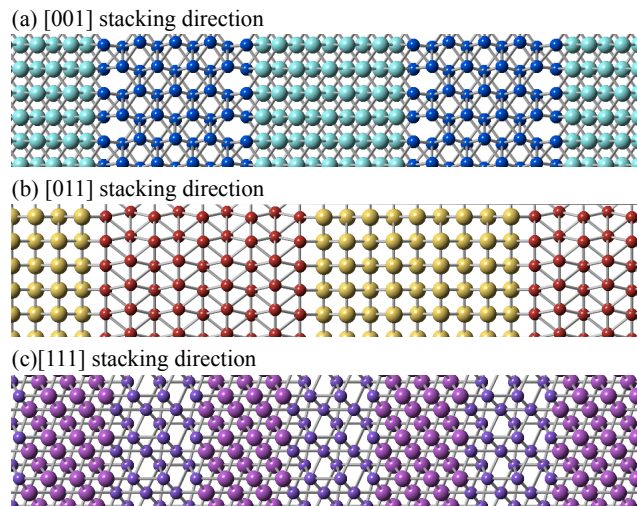(b) [011] stacking direction

(c)[111] stacking direction

FIG. 1. (color online) Geometries of optimized Ti/W superlattices with 9 Ti and 9 W monolayers for (a) [001], (b) [011], and (c) [111] stacking. Small and large spheres represent the Ti and W atoms, respectively. For all stacking directions the W atoms' local environment remains essentially bcc-like, while a displacement of the Ti atoms away from bcc-like toward hcp-like or ω-like becomes apparent in the core of the Ti layer. The displacements occur perpendicular to the [001] and [011] stacking directions (toward hcp) and parallel to the [111] stacking direction (toward ω).

III. RESULTS

Figure 1 illustrates how the stacking direction of the Ti/W superlattice prods the core of the Ti layer into either a hcp- or ω-like structure. The W atoms retain a bcc-like structure. The W atoms adjacent to the Ti layer show no sign of the pure element's surface reconstruction and in fact impress a bcc-like environment upon the Ti atoms neighboring the W layer. The remaining Ti atoms' displacements occur perpendicular to the [001] and [011] stacking directions toward hcp and parallel to the [111] stacking direction toward ω. The superlattices orient the hcp Ti [1120] axis parallel to bcc W [001], hcp Ti [0001] parallel to bcc W [011], and ω-Ti [0001] parallel to bcc W [111]. Ti layers of a only a few atomic layer thickness remain essentially bcc like.

Figure 1 reveals how strongly the stacking direction affects the superlattice period length. The superlattices with [111] stacking stand out with the clearly shortest period lengths, approximately a factor of $\sqrt{3}$ smaller than those with [001] stacking and roughly a factor of $\sqrt{6}$ smaller than those with [011] stacking. Correspondingly, atoms in the superlattices with [111] stacking have as nearest neighbors atoms from different atomic layers, which dramatically affects the formation energy in the W-rich limit (see below).

Pan *et al.* explored an even-extinction phenomenon for Ti/W superlattices with close to equal Ti and W layers in the small 2Θ region of X-ray diffraction patterns.[7] The corresponding effect appears in calculated X-ray diffraction patterns of the relaxed Ti_9/W_9 superlattices with all stacking directions considered here.

Pan *et al.* also explored the high-angle region near near $2\Theta \approx 40°$, which probes smaller-scale distances including the spacing between {011} planes of bcc W, {002} and {011} planes of hcp Ti, and {011} and {110} planes of ω Ti. Figure 2 shows calculated X-ray diffraction patterns near $2\Theta \approx 40°$ for representative Ti/W superlattices explored here. Tungsten-rich superlattices generate diffraction patterns (Fig. 2(a)) that differ little from that of bcc W. Titanium-rich superlattices generate diffraction patterns (Fig. 2(b)) that closely resemble those of hcp Ti (for [001] and [011] stacking) or ω-Ti (for [111] stacking), albeit distorted.

Figure 2(c) shows how intricate the relation to the pure systems can be for the X-ray diffraction pattern of a Ti/W superlattice with equal amounts of W and Ti. Because the X-ray scattering factor of W surpasses that of Ti, only the pattern from tungsten atoms need be considered. The superlattice's diffraction pattern differs significantly from that of perfect bcc W, which exhibits a single large diffraction peak from the {011} planes within the plotted range. Tetragonal strain applied to the bcc W crystal produces side peaks similar to those from the Ti_9/W_9 [001] superlattice. A superlattice layering nine monolayers of this strained bcc W crystal with an equally thick vacuum layer (SL1) slightly broadens the side peaks and produces an additional peak at $42.5°$. Such a W_9/vacuum superlattice has a period length 0.65 Å shorter than that of the relaxed Ti_9/W_9 superlattice; and indeed, an expansion of the vacuum layer by 0.65 Å (SL2) shifts the large main peak and the satellite peak to positions in agreement with the Ti/W superlattice.
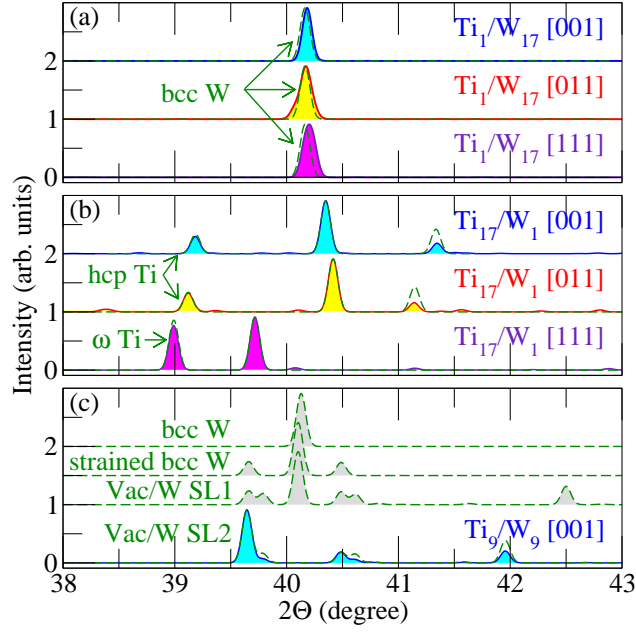
FIG. 2. (color online) Calculated diffraction patterns for Ti/W superlattices. Solid lines represent Ti/W superlattices, dashed lines represent systems with only Ti or W. (a) The diffraction patterns for W-rich superlattices closely approximate the [011] peak of bcc W (with $a = 3.17$ Å). (b) The diffraction patterns for Ti-rich superlattices resemble those of strained hcp and ω-Ti. (c) The diffraction pattern for the Ti_9/W_9 [001] superlattice centers around a large peak at $40.1°$ stemming from $\{019\}$ planes in a tetragonally strained bcc W system. This pattern changes little when nine monolayers of the strained bcc W alternate with a vacuum layer of the same thickness (SL1); the large peak shifts to $39.6°$ only when the strained bcc W appears as part of a superlattice (SL2) with the same period as the Ti_9/W_9 [001] superlattice.
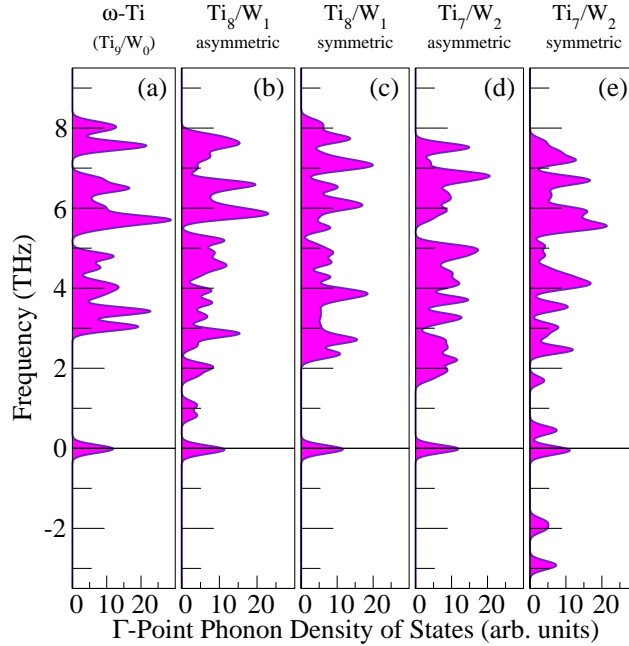

FIG. 3. (color online) Calculated gamma-point phonons for Ti/W superlattices with [111] stacking, nine ($n_{Ti} + n_W = 9$) monolayers, and two atoms per monolayer. The frequencies are plotted with a Gaussian smearing of 0.02 THz. (Each superlattice unit cell corresponds to three stacked ω-Ti unit cells with some Ti atoms replaced by W and allowed to relax.) (a) Titanium in the ω structure. (b) ω-Ti with one of two atoms in a honeycomb layer replaced by W. (c) ω-Ti with one hexagonal layer replaced by W. (d) ω-Ti with W replacing a hexagonal layer and one of two atoms in an adjacent honeycomb layer. (e) ω-Ti with a honeycomb layer replaced by W.
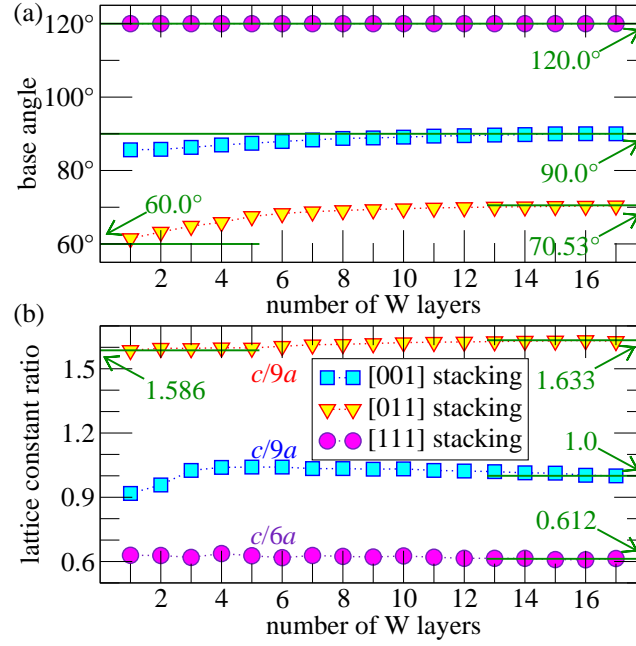
FIG. 4. (color online) Optimized unit cell parameters for 18 atomic layer Ti/W superlattices as a function of number of W atomic layers. (a) The in-plane lattice vectors span the base angle. (b) The lattice constant ratio compares the lattice constant in the stacking direction to the in-plane lattice constant; the plotted ratios are divided by nine for [001] and [011] stacking and by six for [111] stacking. Dotted lines serve to guide the eye. Horizontal lines indicate the ideal values of the unit cell parameters for the bcc and hcp structures at the W-rich and Ti-rich ends, respectively.

As noted above, the unit cells with one atom per monolayer for [111] stacking prove to be too restrictive. Allowing two (or more) atoms per monolayer reveals that a thick enough W layer destabilizes the ω-Ti layer of the superlattice. Full relaxation of these unstable superlattices dramatically reshapes the supercells and drives them toward superlattices with all atoms in a bcc-like environment and short period lengths (computationally, the most favorable superlattice with equal Ti and W layer thicknesses Ti_n/W_n has $n = 2$). The structure illustrated in Fig. 1(c) remains mechanically stable only for three cases (see Fig. 3): the pure Ti limit (ω-Ti), ω-Ti with a monatomic thin W layer, or ω-Ti with a two-monatomic W layer with asymmetric placement of the W atoms (i.e., the W atoms replace a hexagonal layer and one half of a neighboring honeycomb layer). The superlattice becomes unstable if a Ti honeycomb layer is fully replaced by W atoms or if more than two Ti monolayers are substituted. The lack of imaginary phonon frequencies for ω-Ti reflects the phase's metastability, i.e., the finite energy barrier between the ω and hcp phases in pure Ti.[20]

The unstable phonon modes show that, in general, superlattices that layer bcc W with ω-Ti do not exist. However, unit cells with one atom per monolayer prevent such systems from following the unstable phonon modes and are used below to study the properties of such artificial superlattices. These prove to be interesting because they reveal tendencies that may be of more practical relevance for chemically-related superlattices.

The superlattices that layer bcc W with hcp Ti remain stable, hence unit cell size is not an issue. Therefore, unit cells with only one and two atoms per monolayer for [011] and [001] stacking, respectively, are used in the calculations of the properties described below.

Figure 4 shows how the unit cell parameters depend on the superlattice stacking direction and the number of W monolayers. For all systems the volume monotonically decreases toward the W-rich end. For stacking in the [001] direction, the unit cell retains essentially bcc-like parameters; the base angle between in-plane lattice vectors remains close to $90°$ with a slight decrease for Ti-rich systems, and the scaled lattice constant ratio remains close to unity until it drops off at the Ti-rich end to accommodate the smaller Ti-Ti bonds. For stacking in the [011] direction, the structure smoothly changes from bcc-like at the W-rich end to hcp-like at the Ti-rich end; the base angle remains close to the bcc value for systems with more W than Ti and gradually decreases toward the hcp value for Ti-rich systems. For stacking in the [111] direction, the local changes within the Ti layer occur without changing the base angle and c/a ratio as for the other stacking directions.

Figure 5 shows how the formation energy depends on the superlattice stacking direction and the number of W layers. With few exceptions, the superlattice formation energies fall within an energy range of ±27 meV/atom around zero, indicating that at room temperature they are thermodynamically accessible. Indeed, Pan *et al.* report no difficulties
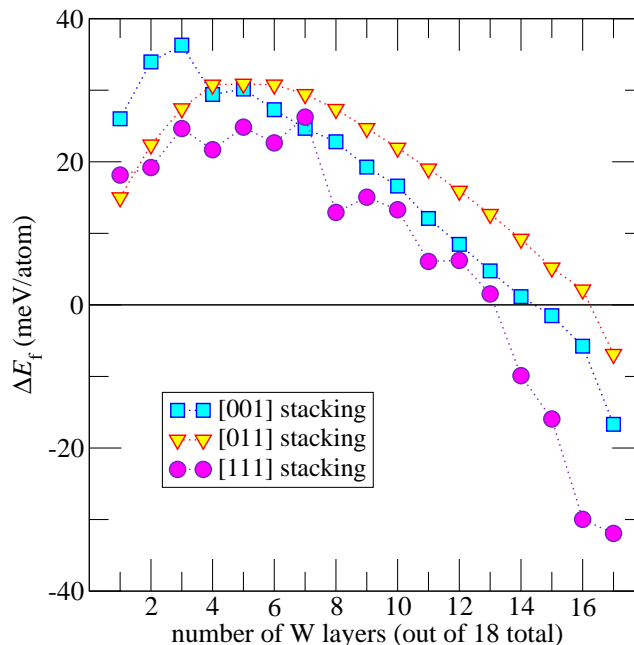
FIG. 5. (color online) Calculated formation energy for 18 atomic layer Ti/W superlattices as a function of number of W atomic layers. The formation energy describes the energy needed to form the superlattices relative to bcc W and hcp Ti. Dotted lines serve to guide the eye.

in their efforts to fabricate Ti/W superlattices.[7–9] All stacking directions favor W-rich superlattices in agreement with experiment: Ti dissolves more easily in W than vice-versa.

Details in the formation energy's dependence on superlattice stacking direction and the number of W layers can be understood from structural specifics. For [001] stacking, superlattices with up to three W monolayers show formation energies that appear shifted upward from that of the other superlattices, this shift arises from the unit cell's departure from bcc-like parameters evident in Fig. 4. The step-like behavior of the formation energy for [111] stacking stems from how well "unit cells" of ω-Ti (with nearly complete plane collapse into a honeycomb layer) can be accommodated within the Ti layer.

The superlattices with [111] stacking exhibit significantly lower formation energies at the W-rich end. This bias can be understood by inspecting the titanium atoms' local environment: For [111] stacking with a single monolayer of Ti, the Ti atoms' nearest neighbors are all W, for two monatomic Ti layers, the Ti atoms' nearest neighbors are 3/8 Ti and 5/8 W, etc. Not until a thickness of five monatomic Ti layers do the central Ti atoms have only Ti nearest neighbors. In superlattices with [001] and [011] stacking, even a single monolayer of Ti has both W and Ti nearest neighbors.

Given the strong influence of the ordered arrangement of Ti and W on the Ti layer's structure in Ti/W superlattices, a strong influence on mechanical properties seems likely. Alloying titanium with randomly placed tungsten particles improves both strength and hardness.[21] The improvement is larger for W atoms dissolved in the Ti matrix than for systems retaining W particles.[22] The superlattices discussed here introduce an alternate, ordered form of "alloying" with its own effects on strength and elasticity. To investigate these effects, incremental tensile strains are applied to the equilibrium superlattice structures in the stacking direction, followed by the relaxation of atomic positions and lattice parameters perpendicular to the stacking direction. Having the perpendicular stresses fall below 0.1 GPa determines convergence.

Figure 6 compares the tensile stress-strain curves calculated for selected Ti/W superlattices and for the elemental systems. For the latter, the strain is applied along the crystallographic direction corresponding to the crystal's orientation parallel to the stacking direction as it appears in the superlattices. In the dilute limits the superlattices behave much like the corresponding pure systems, e.g., [001] stacking with a single W atomic layer exhibits the extreme ductility of α-Ti strained parallel to the [1120] crystallographic direction. Superlattices with equal amounts of Ti and W approximate an average of the pure systems' behaviors.

The ultimate tensile strength of the superlattices tends to fall below those calculated for the pure systems. The Ti-W interface introduces weaker bonds at either the interface or within the Ti layer; none of the strained superlattices failed by breaking bonds between tungsten atoms. Systems that showed bonds breaking within the Ti layer suggests
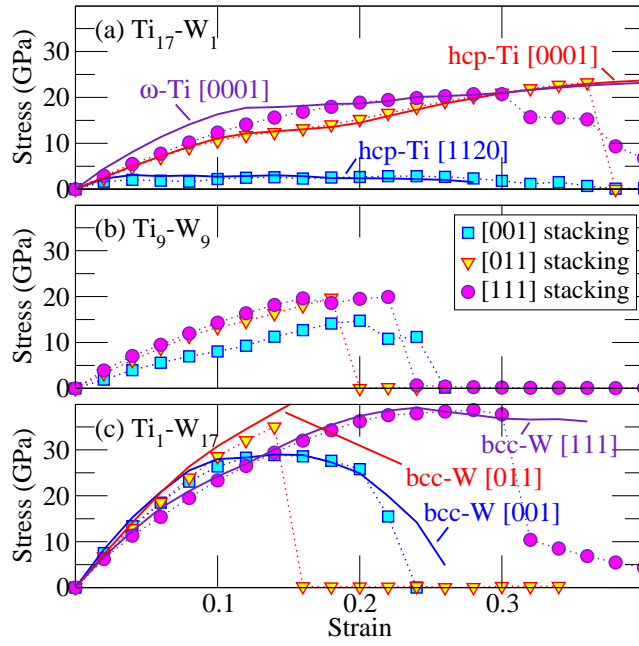
FIG. 6. (color online) Calculated tensile stress-strain curves for 18-atomic layer Ti/W superlattices with (a) one, (b) nine, and (c) seventeen W monolayer(s). For comparison, solid lines show the stress calculated for hcp Ti, ω Ti, and bcc W with strain applied in the crystallographic directions corresponding to their orientation in the superlattices.

axis	Ti_{17}/W_1	Ti_9/W_9	Ti_1/W_{17}	W	Ti	
[001]	82	95	376	415	hcp [11$\bar{2}$0]:	115
[011]	121	162	337	361	hcp [0001]:	130
[111]	145	195	310	333	ω [0001]:	224

TABLE I. Calculated Young's modulus for selected superlattices and elemental systems in units of GPa. Each row lists results for the superlattices with uniaxial strain applied along the stacking direction given in the first column, as well as for the elemental systems strained along the corresponding direction in their crystal structure as oriented within the superlattice layers.

that the effect of the interface on the electronic structure reaches across several monolayers.

Table I lists the Young's moduli evaluated from the initial slope of the tensile stress-strain curves. The values evaluated for the pure systems agree well with the experimental isotropic Young's moduli, 115 GPa for hcp Ti and 410 GPa for bcc W.[23] The moduli for Ti-rich superlattices fall below those of pure Ti, but increase toward the pure W values for the W-rich superlattices. This increase with increased W content differs from systems with evenly distributed W in a Ti matrix, where the addition of W lowers the moduli.[21,22]

These results do not suggest Ti/W superlattices as a means to increase the strength of titanium. The strengthening that results from alloying with randomly placed W particles benefits from separating the W atoms from one another, which suggests that the lack of strengthening in the superlattices stems from the resulting proximity of W atoms, not from their placement being ordered. Even the Ti/W superlattice system with a single W monolayer and [111] stacking, where all nearest neighbors of W atoms are Ti atoms, does not gain strength over the pure Ti system, indicating that improving strength requires W atoms that are well separated throughout the Ti matrix.

IV. CONCLUSIONS

Density functional theory calculations predict that in Ti/W superlattices the W layer remains essentially bcc-like and imparts this structure partway into the Ti layer. The surface reconstruction appearing for pure tungsten does not show up at Ti–W interfaces. The core of the Ti layer becomes hcp-like for [001] and [011] stacking directions. An ω-like Ti layer appears for the [111] stacking direction but becomes unstable if the W layer replaces at least one of the honeycomb layers of the ω-Ti structure. Similar lattice constants of Ti and W make Ti/W superlattices physically

interesting but also make sorting out details in the resulting X-ray diffraction patterns challenging.

The calculated tensile properties of Ti/W superlattices show no improvement over those calculated for the elemental phases. At best, Ti/W superlattices allow a tuning of the material properties by selecting stacking direction and layer thickness.

[1] D. A. Young, *Phase Diagrams of the Elements* (University of California Press, Berkeley, 1991) p. 168.

[2] S. K. Sikka, Y. K. Vohra, and R. Chidambaram, Prog. Mat. Sci. **27**, 245 (1982).

[3] W. Petry, A. Heiming, J. Trampenau, M. Alba, C. Herzig, H. R. Schober, and G. Vogl, Phys. Rev. B **43**, 10933 (1991).

[4] X. Liu, P. K. Chu, and C. Ding, Materials Science and Engineering: R: Reports **47**, 49 (2004).

[5] *Materials Properties Handbook: Titanium Alloys*, edited by G. Welsch, R. Boyer, and E. W. Collings (ASM International, Materials Park, 1994).

[6] *Elements of Metallurgy and Engineering Alloys*, edited by F. C. Campbell (ASM International, Materials Park, 2008) p. 543.

[7] F. M. Pan, J. W. Feng, G. J. Jin, A. Hu, and S. S. Jiang, physica status solidi (b) **195**, 11 (1996).

[8] F. M. Pan, J. W. Feng, G. J. Jin, A. Hu, and S. S. Jiang, Journal of Magnetism and Magnetic Materials **156**, 49 (1996).

[9] F. M. Pan, G. J. Jin, X. L. Wu, J. W. Feng, A. Hu, and S. S. Jiang, Journal of Applied Physics **80**, 4063 (1996).

[10] W. Parrish, Acta Crystallographica **13** (1960).

[11] J. Spreadborough and J. W. Christian, Proceedings of the Physical Society **74**, 609 (1959).

[12] A. Melmed, S. Ceyer, R. Tung, and W. Graham, Surface Science **111**, L701 (1981).

[13] T. Aruga, J. Phys.: Condens. Matter **14**, 8393 (2002).

[14] H.-J. Ernst, E. Hulpke, and J. P. Toennies, Phys. Rev. B **46**, 16081 (1992).

[15] G. Kresse and J. Furthmuller, Phys. Rev. B **54**, 11169 (1996).

[16] G. Kresse and D. Joubert, Phys. Rev. B **59**, 1758 (1999).

[17] P. E. Blöchl, Phys. Rev. B **50**, 17953 (1994).

[18] J. P. Perdew, K. Burke, and M. Ernzerhof, Phys. Rev. Lett. **77**, 3865 (1996).

[19] P. E. Blöchl, O. Jepsen, and O. K. Andersen, Phys. Rev. B **49**, 16223 (1994).

[20] D. R. Trinkle, R. G. Hennig, S. G. Srinivasan, D. M. Hatch, M. D. Jones, H. T. Stokes, R. C. Albers, and J. W. Wilkins, Phys. Rev. Lett. **91**, 025701 (2003).

[21] M. Frary, S. Abkowitz, S. Abkowitz, and D. Dunand, Materials Science and Engineering: A **344**, 103 (2003).

[22] H. Choe, S. M. Abkowitz, S. Abkowitz, and D. C. Dunand, Journal of Alloys and Compounds **390**, 62 (2005).

[23] M. Guinan and D. Steinberg, Journal of Physics and Chemistry of Solids **35**, 1501 (1974).